Biomed Eng Lett (2014) 4:176-185
DOI 10.1007/s13534-014-0137-z

ORIGINAL ARTICLE

A Novel Hybrid Homomorphic Fuzzy Filter for Speckle Noise Reduction

Nagashettappa Biradar, M. L. Dewal and Manoj Kumar Rohit

Received: 1 February 2014 / Revised: 22 April 2014 / Accepted: 17 June 2014

Abstract
Purpose The presence of speckle noise and artifacts make delineation of transthoracic echocardiographic (TTE) images quite difficult and challenging; the edges are to be preserved while removing noise. To address issues, a novel speckle reduction technique is being proposed and analyzed.
Methods Three fuzzy filters based on median and moving average concepts are experimented in homomorphic domain and the best one is further fine tuned for applications on TTE images. The proposed hybrid homomorphic Fuzzy (HHF) filter is the sequential integration of homomorphic fuzzy filter with anisotropic diffusion. The denoising characteristics of HHF filter are compared with ten existing techniques tested in homomorphic and other seven in non-homomorphic domain using seven different performance parameters along with visual quality assessment. Experimentations are performed on TTE images acquired in two parasternal and three apical views, since image in one view may not very precisely speak of underlying valvular abnormality.
Results The edge preservation capability is increased by many fold (around 8 times) upon integration of homomorphic fuzzy filter with the anisotropic diffusion filtering technique. Beta metric, figure of merit and structure similarity indices are all greater than 0.97 for proposed HHF filter.
Conclusions The performance of proposed HHF filter is superior in comparison to seventeen state-of-art denoising techniques in terms of all seven performance parameters. Noise is reduced with the edges and structure of TTE images well preserved.

Nagashettappa Biradar (✉), M. L. Dewal and Manoj Kumar Rohit
Indian Institute of Technology Roorkee, Roorkee-247667, India
Tel : +91-9458129578 / Fax : +91-1132-273560
E-mail : nmbiradar@gmail.com

Manoj Kumar Rohit
Post Graduate Institute of Medical Education and Research, Chandiagarh-160012, India

Keywords Fuzzy filter, Anisotropic diffusion, Speckle reduction, Edge preservation, Echocardiography

INTRODUCTION

Echocardiography, an ultrasound based technique, is the most commonly used first-line imaging technique in the diagnosis and assessment of valvular abnormalities like stenosis and regurgitation of all four valves [1]. It is a noninvasive and clinically handy technique. But low contrast, shadowing artifacts and speckle noise make it extremely tricky to accurately and consistently measure cardiac structure sizes [2, 3]. The speckle noise masks finer lesion details and reduce human visual ability of detecting abnormalities [3, 4]. Multiplicative nature of speckle noise complicates denoising process, as it would not be just enough to remove noise but it is also necessary to preserve the edges in medical images [4, 5].

The omnipresence of multiplicative noise in coherent imaging modalities has lead to development of various types of filters and denoising algorithms. These algorithms are based on principles like Bayesian estimation [6], median and moving average (MAV) [4, 7-9], homomorphic [7, 10], diffusion [11-13], Non-Local means (NLM) [14, 15], and wavelets [5-7, 16]. Each of these filters behave differently with different types of images and noises offering their own advantages and drawbacks, compelling researchers to strive hard to overcome the disadvantages and fine tune each for its variants.

Noise minimization is pronounced using adaptive weighted median (AWM) filter as it adapts to imaging conditions and the functioning of AWM filter depends on the size of the window and the weight adjustment [4, 6, 7, 9]. The other issue with AWM filter is usage of fixed window restricting the enhancement phenomenon and resulting in smeared boundaries [8]. Beta metric (β) for both median and AWM filter decreases with increase in window size and the value of

β is very low (<0.1) [7]. Poor noise removing capability, loss of finer image details, selection of appropriate window size and shape are the basic issues which need to be sorted out in basic techniques [5-8]. The applications of basic noise reduction techniques like median filter and AWM filters are less researched for US images [7, 9]. Fuzzy filters incorporating the concepts of MAV and median filters to define fuzzy membership functions were tested for reducing various types of additive noises [17, 18] but were not tested for multiplicative noise reduction.

Most of multiscale based denoising methods apply a logarithmic transform to translate signal-dependent speckle to additive white noise. These methods result in better additive noise removal and lesser detail loss [5-7]. The choice of appropriate wavelet is the deciding factor for its denoising performance else they introduce artifacts thereby reducing the image quality considerably [6, 7]. In Generalized likelihood ratio filtering method (GLM) using wavelets a single parameter is being utilized for balancing edge preservation in comparison to the amount of noise suppression [16]. The edge balancing parameter is so incorporated as to compensate for the errors induced in the process of estimating the noise standard deviation. In GLM the visual quality of the image is substantially improved in comparison to that using diffusion based methods which give importance to enhancement of edges [16].

Diffusion based methods are known for noise suppression, edge preservation and no induction of artifacts [3, 6, 11] but capability comes under questioning when noise contamination is higher [6]. In order to get rid of limitations of anisotropic diffusion, Yu and Acton [11] proposed speckle reducing anisotropic diffusion (SRAD) technique where gradient based edge discriminator is replaced with a discriminator better suited to speckle [3]. In NLM based denoising, Euclidean distance is computed between the patches and generalization of distance was proposed using iterative probabilistic patches based (PPB) method based on 'Weighted Maximum Likelihood Estimation (WMLE)' [15]. Speaking about the current trends in ultrasound despeckling, Mateo and Fernandez have said that fine tuning and perfecting of basic techniques and their variants is order of contemporary research. The sequential or parallel combinations of the existing techniques may be employed for fine tuning of basic noise reduction techniques [7].

MATERIALS AND METHODS

Based on the background described above, a novel speckle reduction technique based on the sequential combination of homomorphic fuzzy (HF) filter with anisotropic diffusion (AD) is being proposed, tested and analyzed for transthoracic echocardiographic (TTE) images. The proposed sequential mechanism is known as hybrid homomorphic fuzzy (HHF) filter. Further the performance of proposed HHF filter is being compared with seventeen state-of-art denoising techniques comprising of ten methods experimented in homomorphic domain and seven as non-homomorphic methods. The details of these methods are tabulated in Table 1 for quick reference.

Modeling employed for denoising

The multiplicative speckle noise is modeled as

$$f(i,j) = g(i,j)n(i,j) \tag{1}$$

Table 1 Denoising techniques based on different principles.

Author	Method	Type and Modification		Parameter estimated in the Reference paper		Method Number
Bao & Zhang	Products threshold	Wavelet	Log. + Method + Exponential	CNR,MSE	[20]	LOGMPT
Luisier, Blu & Unser	Interscale OWT	Wavelet		PSNR	[21]	LOGOWT
Dengwen & Wengang	NeighShrinkSURE	Wavelet		PSNR	[22]	LOGNSS
Qiao, Song, and Zhao	M-band ridgelet	Ridgelet		PSNR	[25]	LOGMBR
Xu, Yang and Wu	Ripplet NLA	Ripplet		PSNR	[27]	LOGRNLA
Frost, V. S., et al.	Adaptive Wiener	Adaptive		MSE	[19]	LWIF
Kwan and Cai	ATMED, TMAV	Fuzzy		MSE	[18]	HFF
Perona & Malik	PMAD	Diffusion		SNR	[24]	LOGPMA
Weickert	CEAD	Diffusion		SNR	[26]	CEDA
Yu & Acton	SRAD	Diffusion		FOM	[11]	SRAD
Fernandez, Lopez	DPAD	Diffusion		SSIM	[12]	DPAD
Pizurica & Philips	GLM	Wavelet		SNR	[16]	GLM
Coupe, et al.	NLM	NLM		SNR	[14]	NLM
Deledalle, Denis & Tupin	PPB	NLM		SNR	[15]	PPB
Goldstein & Osher	ATV	Total Variation		-	[23]	ATV

IOWT: Interscale orthonormal wavelet thresholding; DPAD: Detail preserving anisotropic diffusion;

Where $g(i,j)$ is noise free image, $f(i,j)$ is the acquired image and $n(i,j)$ is the multiplicative noise, i and j are the variables indicating the spatial locations [7, 10]. The process of converting multiplicative noise to approximated additive noise is performed by taking the logarithm of the input image [7]

$$\log[f(i,j)] = \log[g(i,j)n(i,j)] = \log\{g(i,j)\} + \log\{n(i,j)\} \tag{2}$$

The above Eq. (2) is rewritten with $f_{ij} = \log[f(i,j)]$, $g_{ij} = \log\{g(i,j)\}$ and $n_{ij} = \log\{n(i,j)\}$ as

$$f_{ij} = g_{ij} + n_{ij} \tag{3}$$

This provision using Eq. (3) makes way for application of methods developed for additive white Gaussian noise, to be tested and analyzed on images under the curse of multiplicative noise. In these methods the input is a logarithmic transformed, $f(i,j) = \log(f(i,j))$ and output is being obtained by taking the exponential of denoised image,

$$\hat{g}(i,j) = \exp(MX(\log(f(i,j)))) \tag{4}$$

Where MX stands for denoising methods

Denoising in homomorphic domain

The methods experimented in homomorphic domain were originally designed for additive noise reduction but in this paper they are being experimented for multiplicative noise reduction. Median filter [7], adaptive wiener filter [19], three Fuzzy filter [18], wavelet thresholding techniques [20-22], Ripplet transforms based on non-linear approximation [23], Perona and Malik Anisotropic Diffusion (PMAD), [24], and M-band ridgelet [25] with neighborhood coefficient (NeighCoeff.) thresholding are also being experimented in homomorphic domain for TTE images.

Non-homomorphic denoising methods

Non-homomorphic methods considered for experimentations are NLM [14] and its extension based on PPB filtering [15], diffusion based methods [11, 12, 26], versatile wavelet based denoising based on GLM [16] and anisotropic total variation (ATV) [23]. The limitations of anisotropic diffusion are addressed by SRAD. Diffusion function is controlled by instantaneous coefficient of variation (ICOV) used for edge discrimination [3, 11] and it is defined as given in Eq. (5):

$$\frac{\partial f(i,j;t)}{\partial t} = \nabla.\{c(q).\nabla f(i,j;t)\},\ f(i,j;0) = f_o(i,j) \tag{5}$$

and ICOV is defined by the Eq. (6) [3, 11] given below:

$$q(i,i;t) = \sqrt{\frac{(0.5)\left(\frac{\nabla f}{f}\right)^2 - (0.25)^2\left(\frac{\nabla^2 f}{f}\right)^2}{[1+(0.25)]\left(\frac{\nabla^2 f}{f}\right)^2}} \tag{6}$$

Where ∇^2 is the Laplacian operator and the diffusion function used is of the form defined in Eq. (7) [3, 11]

$$c[q(i,j;t), q_0(t)] = \left(1 + \frac{q^2(i,j,t) - q_0^2(t)}{q^2(i,j,t)(1+q_0^2(t))}\right)^{-1} \tag{7}$$

Where q_0 is the 'speckle scale function'.

The parameters and their values considered in both homomorphic and non-homomorphic techniques are application specific as proposed by the individual authors. In the present paper, all methods are analyzed for images acquired in parasternal and apical views.

Fuzzy filters

Non-linear fuzzy based filtering techniques work based on different membership functions. Fuzzy membership speaks about the degree of similarity and belongingness of an element to a fuzzy set. Three Fuzzy filters based on membership functions incorporating the concepts of median and MAV filters are being tested and analyzed in homomorphic domain and are represented as HF filters. Weighted median filter (WMF) effectively suppresses the speckle noise but the edges are not well preserved [17, 18], however Fuzzy filters preserve image sharpness and the edges when used for denoising of additive noise. Fuzzy filter based on triangular function with median value (TMED), asymmetrical TMED (ATMED) and MAV value with triangular function (TMAV) are formulated in Eqs. (8-9, 10 and 11 and 12), respectively, as described in [17, 18]

$$F[f(i+r,j+s)] = \begin{cases} 1 - \dfrac{|f(i+r,j+s) - f_{med}(i,j)|}{f_{mm}(i,j)}, & for\ |f(i+r,j+s) - f_{med}(i,j)| \le f_{mm}(i,j) \\ 1, & for\ f_{mm} = o \end{cases} \tag{8}$$

$$f_{mm}(i,j) = \max[f_{\max}(i,j) - f_{med}(i,j), f_{med}(i,j) - f_{\min}(i,j)] \tag{9}$$

$$F[f(i+r,j+s)] = \begin{cases} 1 - [f_{med}(i,j) - f(i+r,j+s)] / f_{med}(i,j) - f_{\min}(i,j), \\ \quad for\ f_{\min}(i,j) \le f(i+r,j+s) \le f_{med}(i,j) \\ 1 - [f(i+r,j+s) - f_{med}(i,j)] / [f_{\max}(i,j) - f_{med}(i,j)], \\ \quad for\ f_{med}(i,j) \le f(i+r,j+s) \le f_{\max}(i,j) \\ 1, \quad for\ f_{med}(i,j) - f_{\min}(i,j) = 0\ or\ f_{\max}(i,j) - f_{med}(i,j) = 0 \end{cases} \tag{10}$$

$$F\left[f(i+r,j+s)\right]=\begin{Bmatrix}1-\left|f(i+r,j+s)-f_{mav}(i,j)\right|/f_{mv}(i,j),\\ for\left|f(i+r,j+s)-f_{mav}(i,j)\right|\le f_{mv}(i,j)\\ 1,\ for\ f_{mv}=o\end{Bmatrix} \tag{11}$$

$$f_{mv}(i,j)=\max[f_{\max}(i,j)-f_{mav}(i,j),f_{mav}(i,j)-f_{\min}(i,j)] \tag{12}$$

Where maximum, minimum, median value and moving average value are respectively represented by $f_{\max}(i,j)$, $f_{\min}(i,j)$, $f_{med}(i,j)$ and $f_{mav}(i,j)$ with $s,r\in A$, the window at indices (i,j). The output of the fuzzy filter is given by Eq. (13) [17, 18]

$$y(i,j)=\frac{\sum_{(r,s)\in A}F[f(i+r,j+s)].f(i+r,j+s)}{\sum_{(r,s)\in A}F[f(i+r,j+s)]} \tag{13}$$

Where $F[f(i,j)]$ is general window function and A is the window area. The range of r and s are defined as $-R\le r\le R$ and $-S\le s\le S$ with $N=2R+1=2S+1$, $N*N$ being the window dimensions.

Proposed hybrid Fuzzy filter

Fuzzy filter in the homomorphic domain are being fine tuned by sequentially combining them with SRAD, embedding advantages of both the filters. The proposed hybrid homomorphic fuzzy filtering technique along with all homomorphic and non-homomorphic methods is depicted in Fig. 1, highlighting basic steps involved in the implementation. Each input TTE image is transformed into the logarithmic space according to Eq. (2) and MAV values are calculated using TMAV defined by Eqs. (11-12). The output of the fuzzy filter is estimated using Eq. (13) and exponential operation is performed to bring back the image to non-logarithmic domain using Eq. (4). The output of homomorphic fuzzy filter with TMAV is taken as input to anisotropic diffusion filter resulting in fine tuned denoised image. The steps performed in the proposed method are shown in Fig. 1.

Database

The TTE images are acquired using Philips I33 machine with S5 probe at echo laboratory, Postgraduate Institute of Medical Education and Research (PGIMER), Chandigarh. The study on analysis of echocardiographic images is being approved by Institute Ethic Committee (IEC), PGIMER. In the present experimentation only B-mode images acquired in parasternal long axis (PLAX), parasternal short axis (PSAX), apical four chamber (A4C), apical five chamber (A5C), and apical two chamber (A2C) are being tested. Twenty images were selected in each view during systole and diastole respectively.

RESULTS AND DISCUSSION

The denoising performance of proposed HHF filter along with homomorphic and non homomorphic methods are carried out by evaluating traditional parameters, viz., peak signal to noise ratio (PSNR), mean square error (MSE), correlation coefficient (ρ), and signal to noise ratio (SNR) using original images f_{ij} and denoised images g_{ij} [3, 6, 7]. These parameters speak about the amount of noise reduced in the processed. The edge preservation and distortion of processed images is measured using Prat's Figure of merit (FOM), β, and structural similarity (SSIM) indices [3, 7, 13]. These parameters are expressed as follows:

$$\text{PSNR}=20\times\log(255/\sqrt{\text{MSE}(f_{ij},g_{ij})}) \tag{14}$$

$$\text{MSE}=\frac{1}{MN}\sum_{i=1}^{M}\sum_{j=1}^{N}(f(i,j)-g(i,j))^2 \tag{15}$$

$$\text{SNR}=10\times\log(\text{var}(f_{ij})/\text{MSE}(f_{ij},g_{ij})) \tag{16}$$

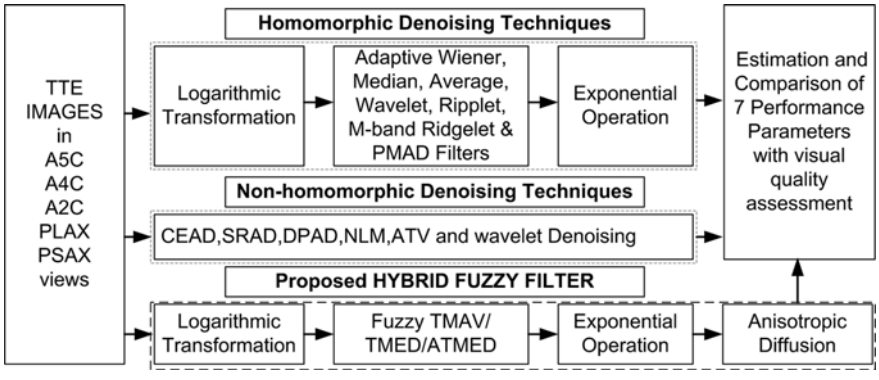

Fig. 1. Homomorphic and Non-homomorphic despeckling techniques.

$$\mathrm{FOM} = \frac{1}{\max(n_d, n_r)} \sum_{j=1}^{n_d} \frac{1}{1+\gamma d_j^2} \tag{17}$$

$$\rho = \frac{\sum_{i=1}^{M}\sum_{j=1}^{N} g_{ij} f_{ij}}{\sqrt{\sum_{i=1}^{M}\sum_{j=1}^{N} g_{ij}^2}\sqrt{\sum_{i=1}^{M}\sum_{j=1}^{N} f_{ij}^2}} \tag{18}$$

$$\beta = \frac{D(\Delta g - \overline{\Delta} g,\ \Delta f - \overline{\Delta} f)}{\sqrt{D(\Delta g - \overline{\Delta} g,\ \Delta g - \overline{\Delta} g).D(\Delta f - \overline{\Delta} f,\ \Delta f - \overline{\Delta} f)}} \tag{19}$$

$$\mathrm{SSIM} = \frac{1}{M} \sum \frac{(2\mu_1\mu_2 + C_1)(2\sigma_{12} + C_2)}{(\sigma_1^2 + \sigma_2^2 + C_2)(\mu_1^2 + \mu_2^2 + C_1)} \tag{20}$$

Where γ is the scalar multiplier being utilized as penalization factor with typical value 1/9, n_d and n_r are the number of pixels in original and processed images respectively, d_j is the Euclidean distance, Δg and Δf represent the filtered version of original and processed images, estimated using Laplacian estimation with a 3×3 pixel approximation, σ_1,σ_2 and μ_1,μ_2 are the standard deviations and means of TTE images compared, σ_{12} represents the covariance, C_1,$C_2 \leq 1$ are the constants.

The performance of HF filter based on TMED, ATMED and TMAV are first tested and analyzed on standard test images of size of 512 × 512 each. Speckle noise is added to the standard test images using MATLAB inbuilt function imnoise with noise variance 0.01-0.3. All experimentations are being performed using MATLAB R2008a. Results obtained for two standard test images in-terms of PSNR, SSIM and FOM are tabulated in Table 2. The results show that the performance of homomorphic fuzzy filter based on ATMED is superior to that of other techniques in terms of traditional denoising performance metrics (PSNR, MSE and SNR).

It is also observed that SSIM and FOM for HF filter based on TMAV are superior in comparison to HF filter based on TMED and ATMED concepts. The higher values of SSIM and FOM indicate lesser distortion and higher edge preservation in the denoised images using HF filter with TMAV. Hence, HF filter with TMAV is considered in further experimentations and is refined using anisotropic diffusion in a sequential fashion. Similar experiments are carried on TTE images but no noise is added to echocardiographic images and it is observed that the results are similar to those quoted above for standard test images.

Results obtained using proposed HHF filter are being compared with HF filter using TMAV and SRAD filter in terms of quantitative parameters in Fig. 2 and visual quality comparisons in Fig. 3. Traditional performance parameters (PSNR, MSE, SNR and ρ) for hybrid homomorphic fuzzy filter are superior in comparison to homomorphic fuzzy filter and SRAD filter. The average of PSNR for HHF filter is higher by 3.7 dB compared to SRAD filter and 9.3 dB for HF filter. MSE is 8 times lesser for HHF filter compared to HF filter and 3.6 times lesser compared to anisotropic diffusion filter. The correlation coefficient value is on an average 0.04 and 0.01 higher compared to HF filter and SRAD respectively. SNR is higher by 1.7 times and 2.5 times respectively compared to that of SRAD and HF filter.

Observing the β value in Fig. 2 reveals that β<0.2 for HF filter and β>0.92 for HHF filter which reveals that β value is increased by 9 times using proposed HHF filter in comparison to HF filter and it is 1.14 times higher compared to SRAD filter.

Visual quality assessments are performed using Fig. 3 and it is observed that the overall structure of the images are well preserved using proposed HHF filter. All the seven parameters (β, FOM, SSIM, ρ, PSNR, MSE and SNR) are superior using proposed HHF filter technique in comparison to both HF filter with TMAV and SRAD filter. Further denoising

Table 2. Performance parameters comparison for standard test images.

Image	Noise variance	Homomorphic Fuzzy Filtering Methods based on ATMED,TMED and TMAV								
		PSNR(dB)			SSIM			FOM		
		ATMED	TMED	TMAV	ATMED	TMED	TMAV	ATMED	TMED	TMAV
Lena	0.01	**30.66**	27.28	29.98	0.8756	0.8657	**0.9217**	0.7349	0.7252	**0.9102**
	0.05	25.28	23.25	**26.25**	0.6787	0.6928	**0.7947**	0.4199	0.4166	**0.5338**
	0.1	**22.51**	19.30	22.34	0.5685	0.5666	**0.6856**	0.3685	0.3573	**0.4082**
	0.2	**19.19**	14.36	17.00	0.4488	0.3915	**0.5048**	0.3295	0.3133	**0.3448**
Monarch	0.01	**27.79**	20.63	23.55	**0.8499**	0.6737	0.8163	**0.9424**	0.9014	0.9166
	0.05	26.15	23.80	**27.01**	0.7747	0.7886	**0.8640**	0.4747	0.5103	**0.6586**
	0.1	**23.09**	19.70	22.75	0.6800	0.6758	**0.7757**	0.4070	0.3848	**0.4908**
	0.2	**19.64**	14.72	17.39	0.5612	0.4927	**0.6094**	0.3322	0.3061	**0.3566**
	0.3	**17.27**	11.26	13.39	**0.4785**	0.2977	0.4139	0.3110	0.2683	0.2938

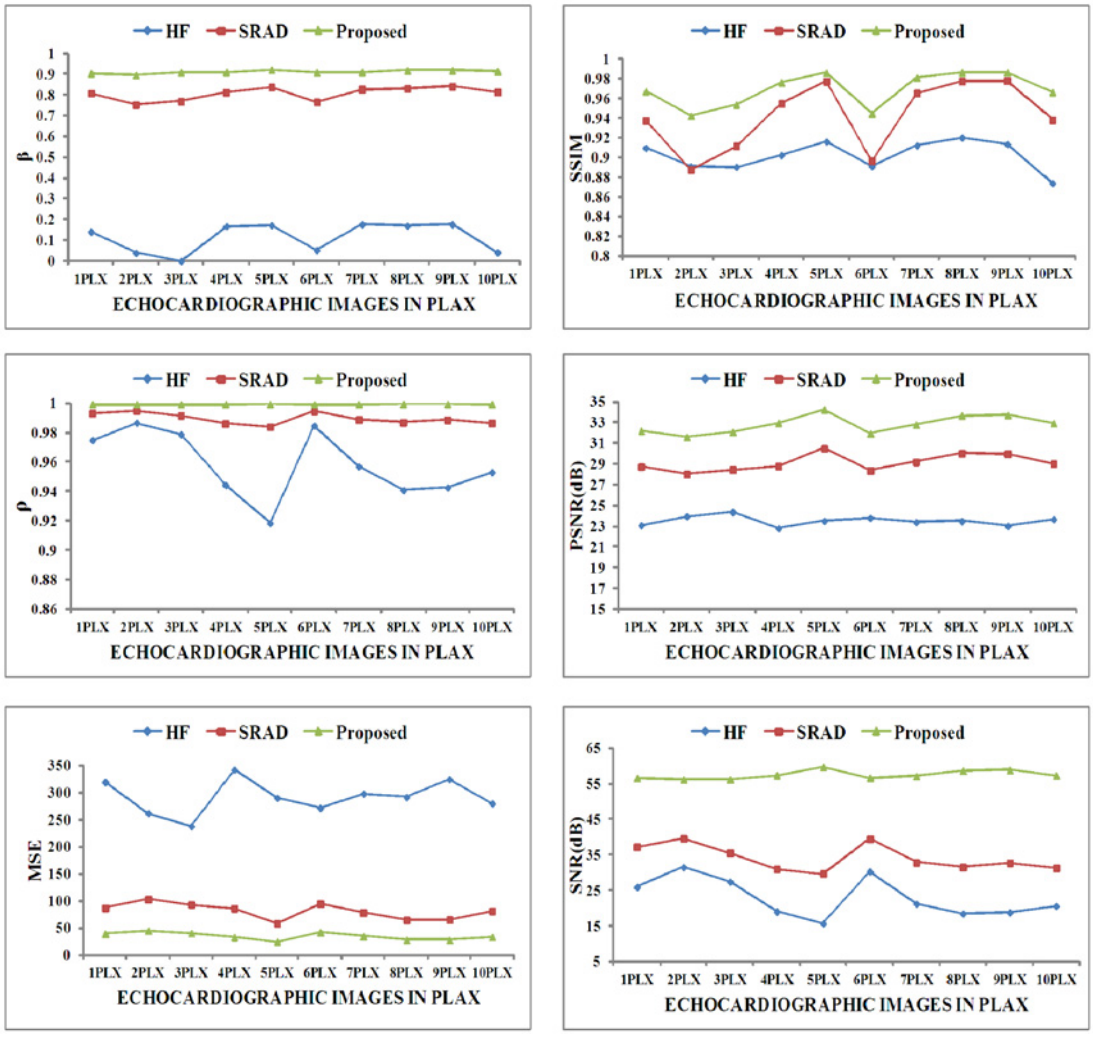

Fig. 2. Performance parameter comparison for TTE images acquired in PLAX using HF, SRAD and proposed filter.

Table 3. Comparison of performance using β and FOM.

Method number	β					Method number	FOM				
	PLX	PSX	A2C	A4C	A5C		PLX	PSX	A2C	A4C	A5C
LOGOWT	0.4363	0.5158	0.4964	0.3945	0.4114	ATV	0.8338	0.8382	0.7736	0.8648	0.8311
LOGAVG	0.4482	0.4726	0.4617	0.4449	0.4564	LOGMPT	0.9025	0.9376	0.9130	0.9369	0.9276
LOGPMA	0.5609	0.5589	0.5581	0.5561	0.5516	HFF	0.9142	0.9145	0.8828	0.8753	0.9312
SRAD	0.8349	0.8156	0.8170	0.8298	0.8299	GLMF	0.9170	0.9179	0.9316	0.9487	0.8934
LOGMPT	0.8669	0.8856	0.8734	0.8717	0.8726	LOGOWT	0.9268	0.9314	0.9435	0.9155	0.9534
LOGRNLA	0.9065	0.8881	0.8881	0.8775	0.9081	LOGAVG	0.9316	0.9311	0.9059	0.9411	0.9241
LWIF	0.9240	0.9254	0.9203	0.9242	0.9174	NLM	0.9493	0.9450	0.9403	0.9781	0.9576
LOGNSS	0.9302	0.9426	0.9377	0.9396	0.9364	PPB	0.9520	0.9696	0.9577	0.9529	0.9583
NLM	0.9385	0.9390	0.9334	0.9378	0.9400	LOGMED	0.9539	0.9444	0.9351	0.9639	0.9382
ATV	0.9433	0.9509	0.9441	0.9457	0.9416	LWIF	0.9559	0.9547	0.9249	0.9584	0.9445
PPB	0.9522	0.9524	0.9490	0.9500	0.9477	LOGNSS	0.9610	0.9753	0.9690	0.9757	0.9728
GLM	0.9669	0.9739	0.9678	0.9707	0.9662	LOGRNLA	0.9614	0.9741	0.9741	0.9580	0.9764
Proposed	**0.9754**	**0.9758**	**0.9750**	**0.9766**	**0.9742**	Proposed	**0.9768**	**0.9800**	**0.9634**	**0.9795**	**0.9679**

quality of HHF filter is being compared with seventeen despeckling methods and visual results are depicted in Fig. 4. The quantitative parameters are tabulated in Tables 3 and 4.

The visual quality of TTE images in PSAX on application of homomorphic and non-homomorphic methods are being compared with HHF filter in Fig. 4. The contrast of images

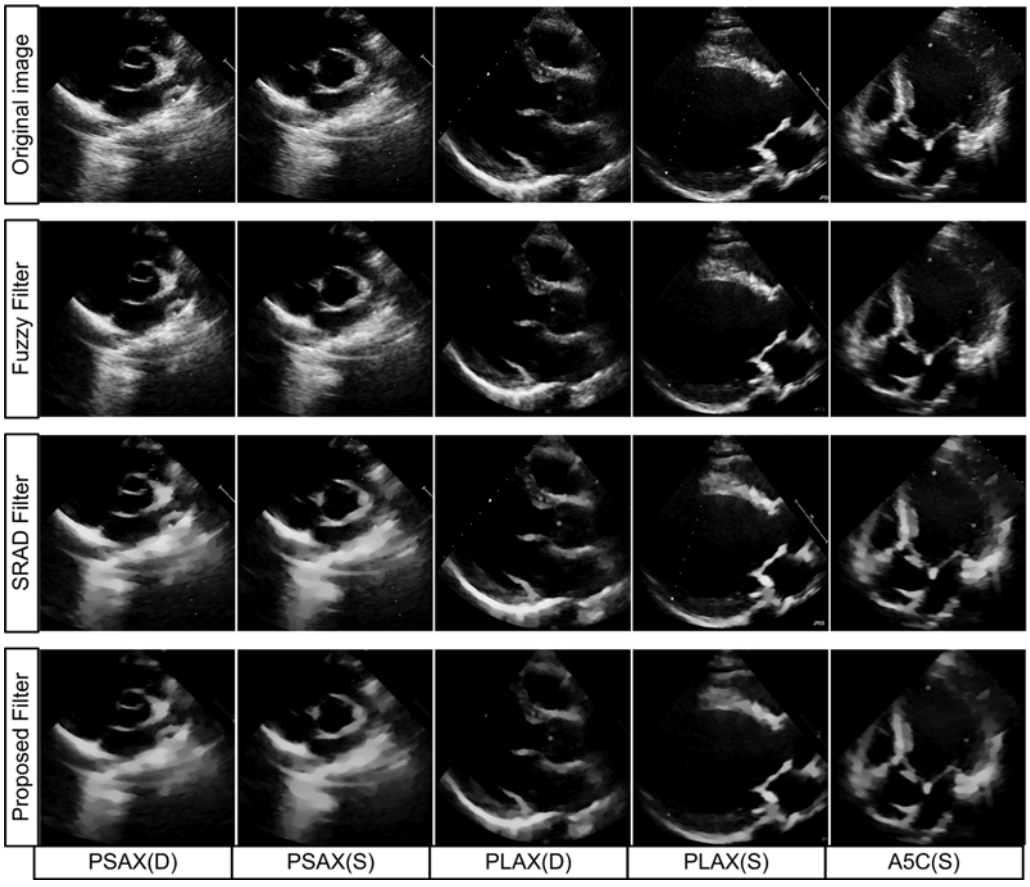

Fig. 3. Visual quality comparison for TTE image denoising using fuzzy, SRAD and proposed filter.

Table 4. Comparison of performance using PSNR and MSE.

Method number	PSNR(dB)					Method number	MSE				
	PLX	PSX	A2C	A4C	A5C		PLX	PSX	A2C	A4C	A5C
DPAD	13.54	15.02	14.15	15.39	14.09	LOGMBR	278.34	310.41	308.76	282.90	303.52
LOGMBR	23.69	23.21	23.23	23.61	23.31	HFF	222.73	207.63	223.51	228.37	209.66
HFF	24.65	24.96	24.64	24.54	24.92	LOGOWT	204.44	131.85	172.73	263.25	260.71
LOGOWT	25.03	26.93	25.76	23.93	23.97	LOGAVG	140.56	150.58	156.87	141.28	148.11
LOGMED	28.75	28.50	28.28	28.66	28.59	LOGMED	86.66	91.89	96.71	88.52	90.04
SRAD	30.96	30.34	30.41	30.54	31.12	SRAD	52.18	60.15	59.16	57.46	50.26
LOGMBR	32.62	33.66	32.91	33.45	33.05	LOGMPT	35.59	27.99	33.25	29.39	32.18
LWIF	34.63	34.20	33.89	34.62	33.94	LWIF	22.41	24.74	26.55	22.43	26.26
ATV	34.83	35.49	34.54	35.37	34.47	ATV	21.37	18.35	22.84	18.89	23.22
LOGRNLA	35.86	35.67	35.67	34.51	36.85	LOGRNLA	16.88	17.63	17.63	23.01	13.42
LOGNSS	36.18	37.57	36.78	37.48	37.07	LOGNSS	15.68	11.37	13.65	11.62	12.76
NLM	36.78	36.72	36.12	36.80	36.65	NLM	13.66	13.85	15.90	13.57	14.07
PPB	37.78	38.10	37.50	38.12	37.40	PPB	10.83	10.08	11.57	10.02	11.82
GLM	38.85	39.85	38.59	39.55	38.63	GLM	8.48	6.74	8.99	7.21	8.92
Proposed	**40.42**	**40.40**	**40.34**	**40.62**	**40.20**	Proposed	**5.90**	**5.93**	**6.01**	**5.64**	**6.20**

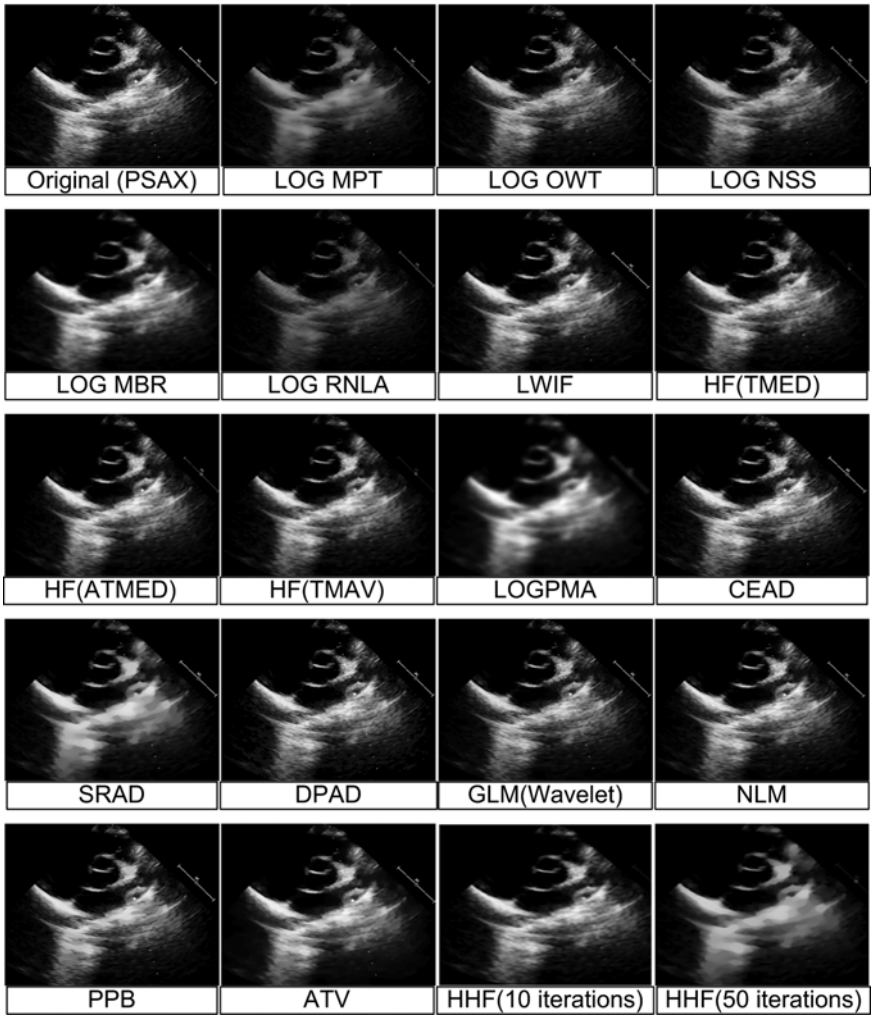

Fig. 4 Visual quality of TTE images after application of homomorphic and non-homomorphic techniques compared to proposed HHF filter.

Table 5. Comparison of performance using and SNR.

Method number	ρ					Method number	SNR(dB)				
	PLX	PSX	A2C	A4C	A5C		PLX	PSX	A2C	A4C	A5C
HFF	0.9518	0.9669	0.9621	0.9584	0.9500	HFF	20.16	23.51	22.29	21.51	19.91
LOGAVG	0.9778	0.9679	0.9718	0.9672	0.9739	LOGMBR	20.97	17.28	18.89	17.36	19.17
LOGMED	0.9860	0.9797	0.9822	0.9787	0.9837	LOGOWT	23.65	24.72	23.94	17.98	20.49
SRAD	0.9887	0.9904	0.9900	0.9896	0.9881	LOGAVG	26.90	23.56	24.78	23.39	25.41
LOGMPT	0.9944	0.9941	0.9941	0.9932	0.9944	LOGMED	31.10	27.85	28.98	27.45	29.73
ATV	0.9967	0.9962	0.9960	0.9957	0.9960	SRAD	32.77	34.27	33.83	33.50	32.31
LWIF	0.9967	0.9953	0.9956	0.9953	0.9958	LOGMPT	38.83	38.18	38.25	37.03	38.67
LOGRNLA	0.9973	0.9961	0.9961	0.9958	0.9968	LWIF	42.85	39.25	40.21	39.37	40.43
LOGNSS	0.9975	0.9975	0.9975	0.9972	0.9977	ATV	43.26	41.85	41.51	40.87	41.50
NLM	0.9978	0.9970	0.9971	0.9968	0.9975	LOGRNLA	45.31	42.19	42.19	41.45	43.84
PPB	0.9983	0.9978	0.9979	0.9976	0.9979	LOGNSS	45.95	46.00	45.98	45.09	46.70
GLM	0.9986	0.9985	0.9984	0.9983	0.9984	NLM	47.15	44.29	44.66	43.74	45.85
Proposed	**0.9994**	**0.9995**	**0.9995**	**0.9995**	**0.9994**	PPB	49.16	47.05	47.42	46.38	47.36
CEAD	**1.0000**	**1.0000**	**1.0000**	**1.0000**	**1.0000**	GLM	51.29	50.55	49.61	49.23	49.81
DPAD	**1.0000**	**1.0000**	**1.0000**	**1.0000**	**1.0000**	Proposed	**58.86**	**59.39**	**59.37**	**59.41**	**58.59**

is reduced using LOGRNLA and LOGPMA and over smoothing is observed using LOGMPT, LOGPMA and LOGMBR. Analysis of results in Table 4 shows that PSNR of the non-homomorphic methods is higher compared to homomorphic methods except in the case of DPAD based filtering. It is higher by more than 1.5 times for proposed HHF filter compared to HF filter, LOGMED, LOGMBR, LOGOWT filters and 1.1 times higher compared to NLM, LOGNSS, LOGRNLA and SRAD based denoising.

It should be noted that PSNR of DPAD method is the lowest among the methods compared and it is 2.8 times lesser compared to HHF filter. All the methods are arranged in increasing PSNR values in Table 4 and it is observed that PSNR for HHF filter is the highest of all other techniques. The MSE values are arranged in decreasing order in Table 4, and it observed that HHF filter has the lowest MSE compared to all other methods. MSE for HF filter and LOGOWT filter are nearly 40 times higher compared to HHF filter.

Observation drawn from Table 5 show that the value of ρ for the proposed HHF filter is higher by 0.01 compared to LOGMED, LOGAVG, LOGMPT, and SRAD filter and 0.04 higher compared to HF filter. The FOM and β are tabulated in Table 3 in increasing order and it is noticed that the highest values of both parameters are achieved using proposed HHF filter technique. Results obtained show that the β value is being doubled using HHF filter in comparison to LOGOWT and LOGAVG. It is also seen that β is higher by 0.1 in comparison to SRAD and LOGMPT and on-par or fractionally superior compared to GLM and PPB based denoising. FOM for HHF filter is fractionally superior or on par in comparison to LOGRNLA, LOGNSS, and LWIF based denoising. The value of FOM is higher compared to all other methods. It is higher by 0.14 compared to ATV, 0.07 compared to LOGMPT, and 0.06 compared to HF filter and GLM filters.

CONCLUSIONS

Three HF filters based on concepts median and moving average filters are tested on TTE images. The results obtained for HF filter based on TMAV are superior in terms of edge preservation and this filter is integrated with anisotropic diffusion sequentially. Denoising performance of the proposed hybrid homomorphic Fuzzy filter is superior in terms of all seven different performance parameters compared to HF filter and SRAD filter for images acquired in two parasternal and three apical views. Edge preservation of HF filter is increased by many fold (around 8 times) using HHF filter. Further the performance is compared with ten methods tested in homomorphic domain and seven in non-homomorphic domain. The seven quantitative performance parameters are on-par or superior for proposed HHF filter with edges and structures well preserved in comparison to all seventeen techniques tabulated.

HUMAN RIGHTS STATEMENTS AND INFORMED CONSENT

All procedure followed were in accordance with the ethical standards of the responsible committee on human experimentation (institutional and national) and with Helsinki Declaration of 1975, as revised in 2000(5). Informed consent was obtained from all patients for being included in the study.

CONFLICT OF INTEREST STATEMENTS

Biradar N declares that he has no conflict of interest in relation to the work in this article. Dewal ML declares that he has no conflict of interest in relation to the work in this article. Rohit MK declares that he has no conflict of interest in relation to the work in this article.

REFERENCES

[1] Kaddoura S. Echo made easy. 2nd ed. London: Elsevier Health Sciences; 2012.
[2] Tenbrinck D, Sawatzky A, Jiang X, Burger M, Haffner W, Willems P, Paul M, Stypmann J. Impact of physical noise modeling on image segmentation in echocardiography. Vis Comput Biol Med. 2012; 33-40.
[3] Finn S, Glavin M, Jones E. Echocardiographic speckle reduction comparison. IEEE T Ultrason Ferroelectr Freq Control. 2011; 58(1):82-101.
[4] Loupas T, McDicken WN, Allan PL. An adaptive weighted median filter for speckle suppression in medical ultrasonic images. IEEE T Circuits Syst. 1989; 36(1):129-35.
[5] Ozcan A, Bilenca A, Desjardins AE, Bouma BE, Tearney GJ. Speckle reduction in optical coherence tomography images using digital filtering. J Opt Soc Am A Opt Image Sci Vis. 2007; 24(7):1901-10.
[6] Wong A, Mishra A, Bizheva K, Clausi DA. General Bayesian estimation for speckle noise reduction in optical coherence tomography retinal imagery. Opt Express. 2010; 18(8):8338-52.
[7] Mateo JL, Fernández-Caballero A. Finding out general tendencies in speckle noise reduction in ultrasound images. Expert Syst Appl. 2009; 36(4):7786-97.
[8] Czerwinski RN, Jones DL, O'Brien Jr WD. Ultrasound speckle reduction by directional median filtering. Conf Proc IEEE Image Process. 1995; 1:358-61.
[9] Qiu F, Berglund J, Jensen JR, Thakkar P, Ren D. Speckle noise reduction in SAR imagery using a local adaptive median filter. GIScience Remote Sens. 2004; 41(3):244-66.
[10] Zong X, Geiser EA, Laine AF, Wilson DC. Homomorphic wavelet shrinkage and feature emphasis for speckle reduction and enhancement of echocardiographic images. Proc Med Imaging: Image Process. 1996; doi:10.1117/12.237969.
[11] Yu Y, Acton ST. Speckle reducing anisotropic diffusion. IEEE T

Image Process. 2002; 11(11):1260-70.
[12] Aja-Fernández S, Alberola-López C. On the estimation of the coefficient of variation for anisotropic diffusion speckle filtering. IEEE T Image Process. 2006; 15(9):2694-701.
[13] Mittal D, Kumar V, Saxena SC, Khandelwal N, Kalra N. Enhancement of the ultrasound images by modified anisotropic diffusion method. Med Biol Eng Comput. 2010; 48(12):1281-91.
[14] Coupé P, Hellier P, Kervrann C, Barillot C. Nonlocal means-based speckle filtering for ultrasound images. IEEE T Image Process. 2009; 18(10):2221-9.
[15] Deledalle C-A, Denis L, Tupin F. Iterative weighted maximum likelihood denoising with probabilistic patch-based weights. IEEE T Image Process. 2009; 18(12):2661-72.
[16] Pizurica A, Philips W, Lemahieu I, Acheroy M. A versatile wavelet domain noise filtration technique for medical imaging. IEEE T Med Imaging. 2003; 22(3):323-31.
[17] Kwan HK. Fuzzy filters for noise reduction in images. In: Nachtegael M, Van der Weken D, Kerre EE, Van De Ville D, editors. Fuzzy Filters for Image Processing. Berlin Heidelberg: Springer. 2003. pp. 24-53.
[18] Kwan H, Cai Y. Fuzzy filters for image filtering. Midwest Symp Circuit. 2002; 3:672-5.
[19] Frost VS, Stiles JA, Shanmugam KS, Holtzman JC, Smith SA. An adaptive filter for smoothing noisy radar images. Proc IEEE. 1981; 69(1):133-5.
[20] Bao P, Zhang L. Noise reduction for magnetic resonance images via adaptive multiscale products thresholding. IEEE T Med Imaging. 2003; 22(9):1089-99.
[21] Luisier F, Blu T, Unser M. A new SURE approach to image denoising: interscale orthonormal wavelet thresholding. IEEE T Image Process. 2007; 16(3):593-606.
[22] Dengwen Z, Wengang C. Image denoising with an optimal threshold and neighbouring window. Pattern Recogn Lett. 2008; 29(11):1694-7.
[23] Goldstein T, Osher S. The split Bregman method for L1-regularized problems. SIAM J Imaging Sci. 2009; 2(2):323-43.
[24] Perona P, Malik J. Scale-space and edge detection using anisotropic diffusion. IEEE T Pattern Anal. 1990; 12(7):629-39.
[25] Qiao Y-L, Song C-Y, Zhao C-H. M-band ridgelet transform based texture classification. Pattern Recogn Lett. 2010; 31(3): 244-9.
[26] Weickert J. Coherence-enhancing diffusion filtering. Int J Comput Vision. 1999; 31(2-3):111-27.
[27] Xu J, Yang L, Wu D. Ripplet: A new transform for image processing. J Vis Commun Image R. 2010; 21(7):627-39.